JOURNAL OF AIRCRAFT
Vol. 40, No. 3, May–June 2003

Aeroelastic Wing with Leading- and Trailing-Edge Control Surfaces

Earl H. Dowell,* Donald B. Bliss,† and Robert L. Clark‡
Duke University, Durham, North Carolina 27708-0300

It is well known that the effectiveness of a trailing-edge control surface can be substantially diminished due to the elastic twist of an airfoil or wing. This aeroelastic phenomenon is known as control surface reversal when the lift or roll rate vanishes at a sufficiently large ratio of flow dynamic pressure to wing stiffness. However, a leading-edge control surface can be used to counteract control surface reversal, and indeed, in principle, a leading-edge control surface may entirely cancel the tendency of the trailing-edge control surface to undergo reversal. Moreover, analysis shows that by using a simple control strategy one can use a combination of leading- and trailing-edge control surface rotations to maintain lift and roll effectiveness and minimize control surface rotations. The beneficial effects of leading-edge control surfaces on control surface reversal are known to practioners. However, the present simple model makes these especially transparent and suggests an advantageous strategy using a combination of leading- and trailing-edge control surfaces.

Introduction

CONTROL surface reversal due to unfavorable aeroelastic effects is one of the classical phenomena of static aeroelasticity. It is treated in textbooks[1,2] and standard courses on aeroelasticity. Here, this well known phenomenon is reconsidered so as to counteract the unfavorable aeroelastic effect associated with trailing-edge control surfaces by a favorable effect of a leading-edge control surface. By an appropriate choice of the ratio of leading- to trailing-edge control surface rotations, a particular advantageous result may be obtained.

To illustrate the concept and fundamental physical phenomena, two simple models are considered: 1) an airfoil and 2) a wing-in-roll. Also, an interesting result for the divergence of a wing-in-roll is highlighted.

The active flexible wing and the active aeroelastic wing programs have been pursued vigorously and reported on widely (for example, Refs. 3–11). A number of important insights and concepts have been highlighted in this literature concerning the effectiveness of multiple control surfaces. These include, most notably, leading-edge control surfaces to offset the traditional loss of effectiveness of trailing-edge control surfaces due to unfavorable aeroelastic wing twist. Noll and Eastep[3] present a cogent overview and organized an issue of the *Journal of Aircraft* on the active flexible wing program. The most directly relevant paper in that issue was by Woods-Vedeler et al.,[4] wherein they discussed various possible control laws to optimize (minimize) roll maneuver loads using active controls.

Later work by Anderson et al.[5] gave deeper insights into the favorable synergy that can be created by a combination of leading- and trailing-edge controls. In their work, they noted that the unfavorable aeroelastic twist that can lead to trailing-edge control surface reversal can be offset by a leading-edge control surface. Moreover, the trailing-edge control surface reversal can be eliminated and a constant roll authority maintained over a wide range of flight dynamic pressures by an appropriate combination of leading- and trailing-edge control surface deflections. In their approach, 1) the (right wing) trailing-edge control surface rotation is trailing-edge down (for rolling to the left) at dynamic pressures below the classical reversal dynamic pressure (for only a trailing-edge control surface in the absence of leading-edge control), 2) then the trailing-edge control surface rotation is set to zero at the dynamic pressure that corresponds to the classical reversal dynamic pressure, and 3) finally the trailing-edge control surface is rotated tail up at yet higher dynamic pressures. The leading-edge control also varies with dynamic pressure, but is always leading-edge nose up with a maximum near the aforementioned classical reversal dynamic pressure. These theoretical trends are consistent with experimental data from a cantilevered wing model of the Agile Falcon.[10]

This is a creative and inventive approach. However, as will be discussed, it appears one can increase the roll rate even beyond that for a rigid wing by an appropriately chosen combination of leading- and trailing-edge control surface deflections. Moreover, as will be seen, the torsional stiffness need not be compromised based on control surface reversal considerations.

More recent work on the active aeroelastic wing concept has dealt with improvements in design optimization methodologies, reduction of drag, and an adaptive change in torsional stiffness to allow both pre- and postclassical reversal operation of an active aeroelastic wing.[6–9] As will be seen, the same conceptual benefit that can be obtained by using a torsional stiffness change can also be realized by using an aeroelastic wing with the gearing ratio between leading- and trailing-edge control surfaces programmed to change with flight dynamic pressure. In Ref. 11, the importance of leading-edge control is also emphasized.

The control strategy to achieve maximum roll performance is straightforward. In the prereversal regime [defined by the classical reversal for a trailing-edge control surface only (no leading-edge control)], the trailing-edge control surface should be at its maximum trailing edge down, and the leading-edge control should be at its maximum nose up. Such a control law minimizes the loss of roll rate due to aeroelastic effects, and indeed, if the leading-edge control surface rotation is sufficiently large, then the roll rate of the aeroelastic wing can exceed that of a rigid wing. However, at a certain flight dynamic pressure, which can be calculated from an appropriate aeroelastic analysis as given in the present paper or determined from a wind-tunnel test of an aeroelastic model, it will be advantageous to reverse the sign of trailing-edge control while maintaining the leading- and trailing-edge control deflections at their maximum values. Note that, in this scheme, the magnitude of the

Received 29 May 2001; revision received 17 May 2002; accepted for publication 20 May 2002.

*J. A. Jones Professor, Department of Mechanical Engineering and Materials Science, Director of the Center for Nonlinear and Complex Systems, and Dean Emeritus, Pratt School of Engineering. Fellow AIAA.

†Associate Professor, Department of Mechanical Engineering and Materials Science, Pratt School of Engineering. Member AIAA.

‡Professor of Mechanical Engineering and Materials Science and Senior Associate Dean, Pratt School of Engineering. Associate Fellow AIAA.

leading- and trailing-edge controls are always maintained at their maximum values at any dynamic pressure to maximize the roll rate, and only the sign of the trailing-edge control surface rotation is changed at a selected and optimized value of dynamic pressure. One can use similar considerations to take into account constraints on wing twist or structural loads because they may affect the control scheme to maximize roll rate. Indeed, one could also determine the control law that would minimize wing twist for a given roll rate or maximum control surface deflection.

Aeroelastic Typical Section Airfoil with Leading- and Trailing-Edge Control Surfaces

Equations of Equilibrium

The equation of torsional equilibrium about the elastic axis follows.[1,2] It expresses the balance of moments about the elastic axis due to the elastic spring and the aerodynamic forces:

$$K_\alpha \alpha = Le + M_{\mathrm{AC}} \tag{1}$$

or

$$K_\alpha \alpha = qc^2[C_L(e/c) + C_{\mathrm{MAC}}] \tag{2}$$

Now define

$$\lambda \equiv qc^2 \big/ K_\alpha \tag{3}$$

a nondimensional ratio of aerodynamic dynamic pressure q to torsional spring stiffness K_α. Here, e is the distance from the aerodynamic center (of lift) to the elastic axis taken as positive when the elastic axis is aft of the aerodynamic center, α is the elastic twist, and c is the airfoil chord.

Then, Eq. (2) becomes

$$\alpha = \lambda[C_L(e/c) + C_{\mathrm{MAC}}] \tag{4}$$

From aerodynamic theory,[1,2] the lift and moment about the aerodynamic center may be expressed as follows:

$$C_L = C_{L\alpha}\alpha + C_{L\eta\,\mathrm{te}}\eta_{\mathrm{te}} + C_{L\eta\,\mathrm{le}}\eta_{\mathrm{le}} \tag{5}$$

where η_{te} is positive trailing edge down and η_{le} is positive leading edge up and

$$C_{\mathrm{MAC}} = C_{\mathrm{MAC}\eta\,\mathrm{te}}\eta_{\mathrm{te}} + C_{\mathrm{MAC}\eta\,\mathrm{le}}\eta_{le} \tag{6}$$

where η_{te} and η_{le} are the trailing- and leading-edge control surface angular rotations and $C_{L\alpha}$, etc., are known (linear theory) aerodynamic coefficients that depend parametrically on Mach number and the wing and control surface planform geometries.

Reversal

By definition, $L = 0$ at reversal. Now using Eqs. (4) in Eq. (6), one may determine the corresponding torsional elastic twist α_R by setting $L = 0$. Thus,

$$\alpha_R = \lambda_R[C_{\mathrm{MAC}\eta\,\mathrm{te}}\eta_{\mathrm{te}} + C_{\mathrm{MAC}\eta\,\mathrm{le}}\eta_{\mathrm{le}}] \tag{7}$$

or

$$\alpha_R = \lambda_R[C_{\mathrm{MAC}\eta\,\mathrm{te}} + rC_{\mathrm{MAC}\eta\,\mathrm{le}}]\eta_{\mathrm{te}} \tag{8}$$

where $r \equiv \eta_{\mathrm{le}}/\eta_{\mathrm{te}}$ is the ratio of leading- to trailing-edge control surface rotations and λ_R corresponds to the reversal dynamic pressure.

Now from Eq. (5),

$$\alpha_R = \frac{-[C_{L\eta\,\mathrm{te}} + rC_{L\eta\,\mathrm{le}}]\eta_{\mathrm{te}}}{C_{L\alpha}} \tag{9}$$

Dividing Eq. (8) by Eq. (9) and rearranging, one has the following expression for λ_R:

$$\lambda_R = \frac{-[C_{L\eta\,\mathrm{te}} + rC_{L\eta\,\mathrm{le}}]}{C_{L\alpha}[C_{\mathrm{MAC}\eta\,\mathrm{te}} + rC_{\mathrm{MAC}\eta\,\mathrm{le}}]} \tag{10}$$

Note that λ_R does not depend on e/c. Also, for $r = 0$, one retrieves the classical reversal result for no leading-edge control surface.[1,2] Finally, note that $\lambda_R \to \infty$ when

$$r = -C_{\mathrm{MAC}\eta\,\mathrm{te}}/C_{\mathrm{MAC}\eta\,\mathrm{le}} \tag{11}$$

Divergence

This is the static instability for which $\alpha \to \infty$ for finite η_{te} or η_{le} or, alternatively, for which α is finite when $\eta_{\mathrm{te}} = \eta_{\mathrm{le}} = 0$. Thus, one may set $\eta_{\mathrm{te}} = \eta_{\mathrm{le}} = 0$ to determine λ_D, the divergence dynamic pressure. When Eqs. (4) and (5) are used,

$$\alpha_D = \lambda_D C_{L\alpha}\alpha_D(e/c)$$

or

$$\lambda_D = 1/C_{L\alpha}(e/c) \qquad \text{for} \qquad \alpha_D \neq 0 \tag{12}$$

Note that λ_D does not depend on η_{te}, η_{le}, or their associated aerodynamic coefficients, and in this linear model, it does not depend on α_D either.

Lift Effectiveness (for General λ)

Now one can determine C_L taking into account twist α of the airfoil and the control surface rotations η_{te} and η_{le} for any λ. First solve for α from Eq. (4), then when Eqs. (5), (6), and (12) are used,

$$\alpha = \lambda/(1 - \lambda/\lambda_D)\{(e/c)[C_{L\eta\,\mathrm{te}} + rC_{L\eta\,\mathrm{le}}] + [C_{\mathrm{MAC}\eta\,\mathrm{te}} + rC_{\mathrm{MAC}\eta\,\mathrm{le}}]\}\eta_{\mathrm{te}} \tag{13}$$

Also Eq. (5) may be rewritten as

$$C_L = [C_{L\alpha}(\alpha/\eta_{\mathrm{te}}) + C_{L\eta\,\mathrm{te}} + rC_{L\eta\,\mathrm{le}}]\eta_{\mathrm{te}} \tag{14}$$

Using Eq. (13) in Eq. (14) and the definitions of λ_R given by Eq. (10) and λ_D given by Eq. (12), one determines that

$$\frac{C_L}{[C_{L\eta_{\mathrm{te}}} + rC_{L\eta\,\mathrm{le}}]\eta_{\mathrm{te}}} = \frac{1 - \lambda/\lambda_R}{1 - \lambda/\lambda_D} \tag{15}$$

The left-hand side of Eq. (15) is the ratio of lift for the aeroelastic airfoil to that for a rigid airfoil. Note that for $r = 0$, one retrieves the classical result for no leading-edge control surface, that is, a trailing-edge control surface only. When $\lambda \to 0$ or $\lambda \ll \lambda_R$ and λ_D, the right-hand side of Eq. (15) approaches unity.

Finally, when $\lambda_R = \lambda_D$, the aeroelastic airfoil lift is equal to the rigid airfoil lift for all λ from Eq. (15). However, note from Eq. (13) that $\alpha \to \infty$ as $\lambda = \lambda_D$ even when $\lambda_R = \lambda_D$. Thus, for the enhancement of lift effectiveness to be useful, one requires that $\lambda < \lambda_D$.

It is of interest to solve for the value of r such that $\lambda_R = \lambda_D$. From Eqs. (10) and (12),

$$r|_{\lambda_R = \lambda_D} = -\frac{[C_{L\eta_{\mathrm{te}}} + \lambda_D C_{L\alpha}C_{\mathrm{MAC}\eta_{\mathrm{te}}}]}{[C_{L\eta_{\mathrm{le}}} + \lambda_D C_{L\alpha}C_{\mathrm{MAC}\eta_{\mathrm{le}}}]} \tag{16}$$

where $\lambda_D \equiv 1/C_{L\alpha}(e/c)$.

One can use Eq. (16) to find a λ_D or e/c such that r has a desired value including $r = 0$. Of course, the smaller the desired r, the smaller is the resulting $\lambda_D (= \lambda_R)$, so that a design optimum will exist that balances a sufficiently large λ_D and not too large a value of r. This optimum depends on the aerodynamic coefficients, of course.

Numerical Results

Typical values of the aerodynamic coefficients are given in Table 1 (see Ref. 12). Control surface chords of 10 and 20% of total airfoil chord are considered for a thin airfoil at $M = 0$. Results for $M \neq 0$ are readily obtained using the Prandtl–Glauert transformation.

Table 1 Aerodynamic coefficients

Coefficients	20%	10%
$C_{\mathrm{MAC}\eta_{\mathrm{te}}}$	−0.64	−0.54
$C_{\mathrm{MAC}\eta_{\mathrm{le}}}$	0.16	0.06
$C_{L\eta_{\mathrm{te}}}$	3.45	2.49
$C_{L\eta_{\mathrm{le}}}$	0.255	0.087

Table 2 $\lambda_{reversal}$ for various r

r	λ_R	λ_R
	20%	10%
0	0.86	0.73
1	1.23	0.86
2	1.97	1.01
3	4.19	1.22
4	∞	——
9	——	∞
−1	0.64	0.64
−2	0.49	0.56

Table 3 $\lambda_{divergence}$ for various e/c

e/c	λ_D
0	∞
0.05	3.18
0.1	1.59

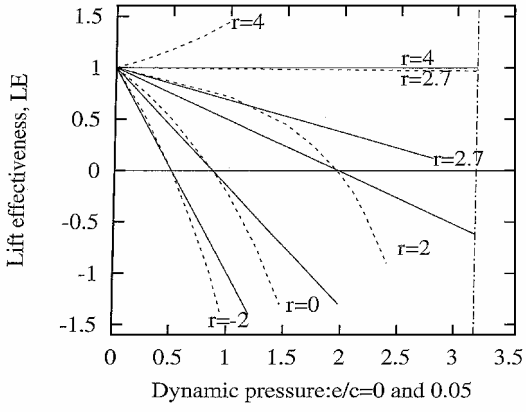

Fig. 1 LE = $C_L/C_{L,rigid}$ vs dynamic pressure λ for $e/c \equiv 0$ (solid line) and 0.05 (broken line): dash-dot line at $\lambda = 3.18 = \lambda_D$ is for $e/c = 0.05$ (note $\lambda_D \Longrightarrow \infty$ as $e/c \Longrightarrow 0$).

Of course, the leading- and trailing-edge control surface chords may be chosen to be different in an optimization design study. Here they are chosen to be the same.

From Eq. (10), we determine the reversal results shown in Table 2.

From Eq. (12), one determines the divergence results shown in Table 3.

Lift Effectiveness Results

When Eqs. (10), (12), and (15) are used, the desired results may be obtained. (Only the case of 20% control surface chords is considered.) These are shown in Fig. 1 for $e/c = 0$ and 0.05. Note that for $e/c \to 0$, dynamic pressure $\lambda_D \to \infty$, and that the variation of lift effectiveness with λ is linear [Eq. (15)].

For any e/c, the results for $r = 0$ are those for no leading-edge control surface. On the other hand, when $r = 2$, for example, the leading-edge control surface rotation is twice that of the trailing edge.

Consider, first, the results for $e/c = 0$. In Fig. 1, it is seen that the lift effectiveness is increased substantially when $r > 0$. The reversal dynamic pressure is increased by over 100% by increasing r from 0 to 2. Note, in particular, that at $\lambda = 0.86$ (corresponding to reversal for $r = 0$), the lift effectiveness is greater than 50% for $r = 2$. Finally, note that above a certain λ (of order 1), it will be advantageous to change the sign of r or the direction of the trailing edge control surface rotation. (See the results for $r = -2$.) Indeed by changing the sign of r above a certain λ, one may achieve a lift effectiveness greater than that for a rigid wing. For $r = -2$, λ_R is reduced, and the aircraft is now operating above the reversal dynamic pressure, that is, $\lambda > \lambda_R$.

Thus, for small λ, one might advantageously select $r > 0$ and operate in the prereversal regime, and for larger λ one might select $r < 0$ and operate in the postreversal regime.

Also for sufficiently large positive r ($r \geq 4$), the lift effectiveness may exceed that of a rigid wing. However for various reasons, such large values of r may be difficult to use in practice.

Now consider the results for $e/c = 0.05$. As expected, λ_R is the same as that for $e/c = 0$ (for any r). Recall Eq. (10). Moreover, as may be expected from an examination of Eq. (15), the lift effectiveness for $e/c = 0.05$ (or any $e/c > 0$) is always greater (in magnitude) than that for $\lambda \neq \lambda_R$. The lift effectiveness becomes very large as $\lambda \to \lambda_D$, that is, $C_L \to -\infty$ (for $r < 4$) or $C_L \to +\infty$ (for $r > 4$). On the other hand, when $e/c < 0$, dynamic pressure $\lambda_D < 0$, and the lift effectiveness will be less than that for $e/c = 0$ for any λ other than $\lambda = \lambda_R$. For $e/c < 0$, the lift effectiveness (LE), as $\lambda \to \infty$, approaches λ_D/λ_R. (Recall that $\lambda_D < 0$ for $e/c < 0$.)

Finally note that, from Eq. (16), when $r = 2.70$, then $\lambda_D = \lambda_R$, and the lift effectiveness is unity for all λ.

Twist Angle Results

For too large a twist angle, the structural integrity of the airfoil or wing may be a concern. Also, aerodynamic stall may become an issue. Thus, it is of interest to compute α. For simplicity set $e/c = 0$ and use Eq. (13) to determine an estimate for α:

$$\alpha|_{e/c=0} = \lambda[C_{\mathrm{MAC}\eta\,\mathrm{te}} + rC_{\mathrm{MAC}\eta\,\mathrm{le}}]\eta_{\mathrm{te}} \tag{17}$$

For typical values of $\lambda \sim 0(1)$ and C_{MAC}, one sees that $\alpha|_{e/c=0}$ is on the order of η_{te} or less. Clearly, in a practical design study, there must be a compromise between competing objectives. However, the twist values seem reasonable for $r > 0$. For $r < 0$, the twist values will be larger, but still not beyond a plausible range of values.

Note that for $r = 4$, the leading- and trailing-edge moments about the elastic axis balance and $\alpha = 0$. However, for such a large r, nonlinear aerodynamic effects (not modeled here) may be important.

Note that, for $e/c > 0$ and $\lambda_D > 0$, the twist will tend to infinity as $\lambda \to \lambda_D$. [Recall Eq. (13).] Thus, the estimate of Eq. (17) is valid for small e/c and/or $\lambda < \lambda_D$, for example, $e/c < 0.1$ and $\lambda/\lambda_D < 0.5$.

One can determine α for any e/c, r, or λ from Eqs. (13).

Aeroelastic Wing-in-Roll with Leading- and Trailing-Edge Control Surfaces

Now consider a straight rectangular wing with leading- and trailing-edge control surfaces that are full span. A more complex geometric planform can be treated using modern computational models.[12]

As will be seen, the results for wing-in-roll, including reversal, divergence, and roll effectiveness, are entirely analogous to those found in the typical section airfoil model. One interesting sidelight of the study is the finding that including the roll degree of freedom greatly increases the (antisymmetric) divergence dynamic pressure. In retrospect, at least, this is not surprising because the rolling moment due to lift must be zero for a constant or steady roll rate. Hence, the lift due to roll rate tends to cancel the lift due to wing twist, and this substantially alleviates the tendency of the aeroelastic wing to diverge as the dynamic pressure increases. Note, however, that the symmetric divergence condition is unchanged.

The torsional equation of equilibrium[1,2] is

$$\frac{\mathrm{d}}{\mathrm{d}y}\left(GJ\frac{\mathrm{d}\alpha}{\mathrm{d}y}\right) + M_y = 0 \tag{18}$$

The aerodynamic model is

$$M_y = eL + M_{\mathrm{AC}} \tag{19}$$

$$L = qcC_L \tag{20}$$

$$C_L = C_{L\alpha}[\alpha - (py/U)] + C_{L\eta\,\mathrm{te}}\eta_{\mathrm{te}} + C_{L\eta\,\mathrm{le}}\eta_{\mathrm{le}} \tag{21}$$

$$M_{\mathrm{AC}} = qc^2C_{\mathrm{MAC}} \tag{22}$$

$$C_{\mathrm{MAC}} = C_{\mathrm{MAC}\eta\,\mathrm{te}}\eta_{\mathrm{te}} + C_{\mathrm{MAC}\eta\,\mathrm{le}}\eta_{\mathrm{le}} \tag{23}$$

Thus, Eqs. (19–23) give

$$M_y = qc^2\{[C_{\mathrm{MAC}\eta\,\mathrm{te}}\eta_{\mathrm{te}} + C_{\mathrm{MAC}\eta\,\mathrm{le}}\eta_{\mathrm{le}}] + (e/c)[C_{L\alpha}[\alpha - (py/U)] + C_{L\eta\,\mathrm{te}}\eta_{\mathrm{te}} + C_{L\eta\,\mathrm{le}}\eta_{\mathrm{le}}]\} \tag{24}$$

where p is the roll rate (angular velocity) and y is the spanwise spatial coordinate.

The rigid-body rolling equations of equilibrium are

$$\int_0^l Ly\,\mathrm{d}y = 0 \tag{25}$$

or

$$\int_0^l \left[C_{L\alpha}\left(\alpha - \frac{py}{U}\right) + C_{L\eta\,\mathrm{te}}\eta_{\mathrm{te}} + C_{L\eta\,\mathrm{le}}\eta_{\mathrm{le}}\right]y\,\mathrm{d}y = 0 \tag{26}$$

Typical Values of the Aerodynamic Coefficients

The aerodynamic coefficients are chosen to be the same as those for the typical section airfoil, that is, a strip theory aerodynamic model is employed. Only control surfaces of 20% chord are considered as an example. Thus,

$$C_{L\alpha} = 2\pi, \qquad C_{L\eta\,\mathrm{te}} = 3.45, \qquad C_{L\eta\,\mathrm{le}} = 0.255$$

$$C_{\mathrm{MAC}\eta\,\mathrm{te}} = -0.64, \qquad C_{\mathrm{MAC}\eta\,\mathrm{le}} = 0.16$$

Solution Procedure

Assume a single structural twist mode,[1,2]

$$\alpha = \bar{\alpha}\sin(\pi y/2l) \tag{27}$$

Substituting Eq. (27) into Eq. (18) and using Eq. (24), multiplying through by $\sin(\pi y/2l)$ and integrating over the wing span, $\int \cdots \mathrm{d}y$ gives the following Galerkin mathematical model:

$$\left[-(\pi/2)^2 + \lambda C_{L\alpha}(e/c)\right]\bar{\alpha} + \lambda\{[C_{\mathrm{MAC}\eta\,\mathrm{te}}\eta_{\mathrm{te}} + C_{\mathrm{MAC}\eta\,\mathrm{le}}\eta_{\mathrm{le}}] + (e/c)[C_{L\eta\,\mathrm{te}}\eta_{\mathrm{te}} + C_{L\eta\,\mathrm{le}}\eta_{\mathrm{le}}]\}(4/\pi) - \lambda C_{L\alpha}(e/c)(8/\pi^2)(pl/U) = 0 \tag{28}$$

Note that, for simplicity, we have taken the control surfaces to be full span and as indicated use strip theory aerodynamics. Refinements to include partial span control surfaces and three-dimensional aerodynamics will not change the essential physical model, although they will clearly be important for design studies.

Also define

$$\lambda \equiv qc^2l^2/GJ$$

Substituting Eq. (27) into (26) gives

$$C_{L\alpha}(12/\pi^2)\bar{\alpha} - C_{L\alpha}(pl/U) + \tfrac{3}{2}[C_{L\eta\,\mathrm{te}}\eta_{\mathrm{te}} + C_{L\eta\,\mathrm{le}}\eta_{\mathrm{le}}] = 0 \tag{29}$$

Consider now some important special cases.

Rigid Wing ($\alpha \equiv 0$)

From Eq. (29) and $\bar{\alpha} = 0$,

$$\frac{pl}{U} = \frac{3}{2}\frac{[C_{L\eta\,\mathrm{te}} + rC_{L\eta\,\mathrm{le}}]\eta_{\mathrm{te}}}{C_{L\alpha}} \tag{30}$$

where

$$r = \eta_{\mathrm{le}}/\eta_{\mathrm{te}} \tag{31}$$

Reversal ($pl/U = 0$)

From Eq. (29), the value of $\bar{\alpha}$ at which reversal occurs may be determined, that is, $\bar{\alpha}_R$:

$$\bar{\alpha}_R = -\frac{3}{2}\frac{[C_{L\eta\,\mathrm{te}} + rC_{L\eta\,\mathrm{le}}]\eta_{\mathrm{te}}}{(12/\pi^2)C_{L\alpha}} \tag{32}$$

From Eq. (28),

$$\bar{\alpha}_R = -\frac{\lambda_R\{[C_{\mathrm{MAC}\eta\,\mathrm{te}} + rC_{\mathrm{MAC}\eta\,\mathrm{le}}] + (e/c)[C_{L\eta\,\mathrm{te}} + rC_{L\eta\,\mathrm{le}}]\}(4/\pi)\eta_{\mathrm{te}}}{\left[-(\pi/2)^2 + \lambda_R C_{L\alpha}(e/c)\right]} \tag{33}$$

Now equating the right-hand sides of Eq. (32) and Eq. (33) and solving for λ_R, we obtain

$$\lambda_R = \left(\frac{\pi}{2}\right)^2 \Big/ C_{L\alpha}\left\{\frac{e}{c}\left[1 - \frac{96}{3\pi^3}\right] - \frac{96}{3\pi^3}\frac{[C_{\mathrm{MAC}\eta\,\mathrm{te}} + rC_{\mathrm{MAC}\eta\,\mathrm{le}}]}{[C_{L\eta\,\mathrm{te}} + rC_{L\eta\,\mathrm{le}}]}\right\} \tag{34}$$

A further special case is $e/c = 0$. Then Eq. (34) reduces to

$$\lambda_R = -\frac{3\pi^5}{384}\frac{[C_{L\eta\,\mathrm{te}} + rC_{L\eta\,\mathrm{le}}]}{C_{L\alpha}[C_{\mathrm{MAC}\eta\,\mathrm{te}} + rC_{\mathrm{MAC}\eta\,\mathrm{le}}]}$$

This is analogous to the result one obtains for lift reversal in the absence of rolling. Note also that the dependence of λ_R on e/c in Eq. (34) is very weak for typical values of e/c and the aerodynamic coefficients.

Divergence ($\eta_{te} = \eta_{le} = 0$)

Setting the determinant of coefficients of $\bar{\alpha}$ and (pl/U) from Eq. (28) and Eq. (29) to zero and solving for $\lambda = \lambda_D$, one obtains

$$\lambda_D = \frac{(\pi/2)^2}{C_{L\alpha}(e/c)(1 - 96/\pi^4)} \tag{35}$$

Note that $\lambda_D = (\pi/2)^2$ is the divergence condition for symmetrical divergence, that is, no roll. Hence, the λ_D with roll included is much higher, and indeed, with roll

$$\lambda_R \ll \lambda_D$$

Compare Eqs. (34) and (35). This greatly increased value for λ_D when roll occurs has presumably been observed by practioners for many years. However, the standard texts[1,2] do not cover this issue, and an admittedly informal and incomplete survey of colleagues has not shown a general awareness of this result. Hancock[14,15] has pointed out that rigid body translation and pitching motions may impact symmetrical divergence.

Roll Effectiveness (General λ)

Solving Eqs. (28) and (29), one obtains

$$pl/U = N_p/D \tag{36}$$

$$\bar{\alpha} = N_\alpha/D \tag{37}$$

where

$$D \equiv \left\{-\left[-(\pi/2)^2 + (e/c)\lambda C_{L\alpha}\right] + (96/\pi^4)(e/c)\lambda C_{L\alpha}\right\}C_{L\alpha} \tag{38}$$

$$N_p \equiv \left\{-\tfrac{3}{2}\left[-(\pi/2)^2 + (e/c)\lambda C_{L\alpha}\right][C_{L\eta\,\mathrm{te}} + rC_{L\eta\,\mathrm{le}}] + (48/\pi^3)\lambda C_{L\alpha}[(C_{\mathrm{MAC}\eta\,\mathrm{te}} + rC_{\mathrm{MAC}\eta\,\mathrm{le}}) + (e/c)(C_{L\eta\,\mathrm{te}} + rC_{L\eta\,\mathrm{le}})]\right\}\eta_{\mathrm{te}} \tag{39}$$

$$N_\alpha \equiv -C_{L\alpha}\left\{-(4/\pi)\lambda[(C_{\mathrm{MAC}\eta\,\mathrm{te}} + rC_{\mathrm{MAC}\eta\,\mathrm{le}}) + (e/c)(C_{L\eta\,\mathrm{te}} + rC_{L\eta\,\mathrm{le}})] + \tfrac{3}{2}(8/\pi^2)(e/c)\lambda(C_{L\eta\,\mathrm{te}} + rC_{L\eta\,\mathrm{le}})\right\}\eta_{\mathrm{te}} \tag{40}$$

Now by the use of Eqs. (35) and (38),

$$D = \left\{\lambda C_{L\alpha}(e/c)[-1 + (96/\pi^4)] + (\pi/2)^2\right\}C_{L\alpha} = (\pi/2)^2 C_{L\alpha}\{1 - (\lambda/\lambda_D)\} \tag{41}$$

and by the use of Eqs. (34) and (39),

$$N_p = \tfrac{3}{2}(\pi/2)^2[C_{L\eta\,\mathrm{te}} + rC_{L\eta\,\mathrm{le}})]\{1 - (\lambda/\lambda_R)\}\eta_{\mathrm{te}} \qquad (42)$$

Thus, from Eqs. (41) and (42), and recalling Eq. (30),

$$\frac{pl}{U}\Big/\frac{3}{2}\frac{[C_{L\eta\,\mathrm{te}} + rC_{L\eta\,\mathrm{le}}]\eta_{\mathrm{te}}}{C_{L\alpha}} = \frac{1-\lambda/\lambda_R}{1-\lambda/\lambda_D} \qquad (43)$$

or roll effectiveness (RE),

$$\mathrm{RE} \equiv \frac{(pl/U)}{(pl/U)_{\mathrm{rigid}}} = \frac{1-\lambda/\lambda_R}{1-\lambda/\lambda_D}$$

Note that one could also determine a dynamic pressure for which $\bar{\alpha} = 0$, that is, $N_\alpha = 0$. At such a dynamic pressure, the roll rate is the same as that for a rigid wing.

Numerical Results

Reversal Results

From Eq. (34), one obtains the results given in Table 4. Note that these results are also quite accurate for any $|e/c| < 0.1$.

Divergence Results

From Eq. (35), one obtains the results given in Table 5. Note that $\lambda_D \gg \lambda_R$ for a rolling wing. Thus, Eq. (43) may be further simplified to

$$\mathrm{RE} \equiv \frac{(pl/U)}{(pl/U)_{\mathrm{rigid}}} \cong 1 - \lambda/\lambda_R \qquad (44)$$

These results are shown graphically in Fig. 2 and are entirely analogous to those for the typical section airfoil. Note, in particular, that an adaptive control strategy where one selects $r > 0$ for small and $r < 0$ for large λ appears attractive. Large λ occurs for large flow dynamic pressure q or small torsional stiffness GJ.

Design Considerations

The full implications for design are many. Here a few key ideas are highlighted. For simplicity, we assume the elastic axis and aerodynamic center coincide, $e/c = 0$, and, thus, $\lambda_D = \infty$. To make the discussion more transparent, recall Eqs. (30) and (34) and rewrite Eq. (44) as follows:

$$\tilde{P} \equiv pl\Big/\frac{3}{2}\sqrt{\frac{2GJ}{\rho c^2 l^2}}\eta_{\mathrm{te}} = \sqrt{\lambda}\left\{\left[\frac{C_{L\eta\,\mathrm{te}}}{C_{L\alpha}} + \lambda\frac{C_{\mathrm{MAC}\eta\,\mathrm{te}}}{3\pi^5/384}\right] + r\left[\frac{C_{L\eta\,\mathrm{le}}}{C_{L\alpha}} + \lambda\frac{C_{\mathrm{MAC}\eta\,\mathrm{le}}}{3\pi^5/384}\right]\right\} \qquad (45)$$

In this form, the explicit dependence of roll rate on the ratio of dynamic pressure to wing torsional stiffness, λ, is seen as well as the individual roles of the trailing- and leading-edge control surfaces. The roll rate is now normalized with respect to a parameter based on wing stiffness, chord, span, and fluid density, as well as control surface rotation η_{te}.

In Eq. (45), the explicit dependence of the trailing-edge control surface contribution to the roll rate on dynamic pressure is clear. Recall the reversal dynamic pressure for the trailing-edge control surface alone is

$$\lambda_R|_{r=0} = \frac{3\pi^5}{384}\frac{C_{L\eta\,\mathrm{te}}}{C_{L\alpha}C_{\mathrm{MAC}\eta\,\mathrm{te}}} \qquad (46)$$

Thus, the contribution of the trailing-edge control surface to the rolling rate changes sign when

$$\lambda > \lambda_R|_{r=0} \qquad \text{or} \qquad \lambda < \lambda_R|_{r=0}$$

Of course, the leading-edge control surface alone does not undergo reversal because the twist due to the leading-edge control surface rotation increases the rolling rate. See the term multiplied by r in Eq. (45).

From the preceding observations based upon Eq. (45), it is clear that one wants to make r as large as possible, and then, when the contribution of the trailing-edge control surface to the roll rate goes to zero as $\lambda \to \lambda_R|_{r=0}$,, reverse the sign of r and η_{te} to maximize the roll rate over the full range of dynamic pressure. This is shown concisely in Fig. 3.

Figure 3 shows the variation of roll rate (normalized by the trailing-edge control surface rotation) with dynamic pressure for a given level of wing torsional stiffness. In the linear aeroelastic model, the roll rate is proportional to the trailing-edge rotation for fixed ratio of leading- to trailing-edge rotations. Thus, the inverse of

Table 4 $\lambda_{\mathrm{reversal}}$ for various r

e/c	r	λ_R
0	0	2.05
0	1	2.94
0	2	4.71
0	3	10.0
0	4	∞
0	5	−11.2
0	−1	1.53
0	−2	1.17

Table 5 $\lambda_{\mathrm{divergence}}$

e/c	λ_D
0	∞
0.1	170

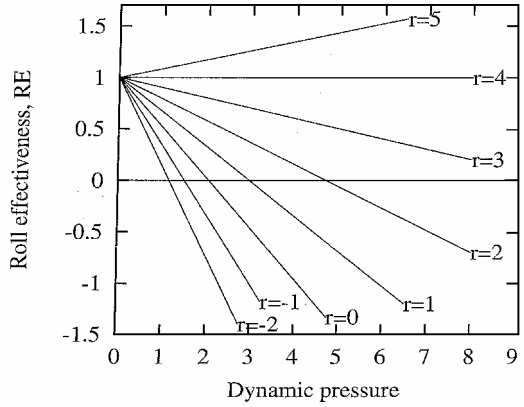

Fig. 2 RE = $(pl/U)/(pl/U)_{\mathrm{rigid}}$ vs dynamic pressure λ: note that $\lambda \equiv qc^2l^2/GJ$, $pl/U = 0 \Rightarrow$ reversal and $r \equiv$ ratio of leading- to trailing-edge control surface rotation.

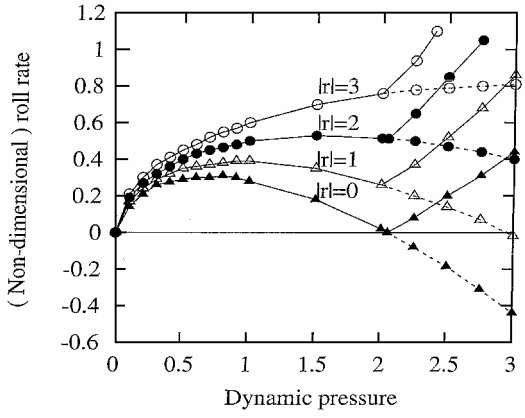

Fig. 3 Nondimensional roll rate vs dynamic pressure λ: comparison of conventional (– – –) vs proposed (——) control strategies.

Fig. 3 may also be interpreted as the trailing-edge rotation required for a given roll rate.

When there is no leading-edge control ($r = 0$), there is a dynamic pressure when the roll rate goes to zero, that is, the reversal dynamic pressure for a trailing-edge control surface only. Of course, for small dynamic pressure and in the limit as the dynamic pressure tends to zero, the roll rate also tends to zero.

With leading-edge control added ($r \neq 0$), reversal is eliminated using the strategy already described. Indeed, for a sufficiently large leading-edge control authority, the roll rate is a monotonically increasing function of dynamic pressure. This result also implies that for a given desired roll rate, the trailing-edge (and leading-edge) control surface rotations needed are monotonically decreasing functions of dynamic pressure. This is an attractive design option because it implies that the leading- and trailing-edge control authority may be determined by low dynamic pressure requirements to achieve desired roll rates.

The value of r for which the dependence of p on λ and vice versa is monotonic may be determined from a further analysis of Eq. (45). It is given by

$$r = 2/[-3(C_{\mathrm{MAC}\eta\,\mathrm{le}}/C_{\mathrm{MAC}\eta\,\mathrm{te}}) + (C_{L\eta\,\mathrm{le}}/C_{L\eta\,\mathrm{te}})] \qquad (47)$$

For the aerodynamic data used herein, $r = 2.43$.

Representative results from Eq. (45) using the proposed control strategy are shown by the solid lines in Fig. 3. Also shown for reference are the results that are obtained when the sign of r is not changed. See the dashed lines in Fig. 3. Clearly using the proposed strategy has a very beneficial effect on the rolling rate.

There is another interesting set of questions regarding the optimum choice of wing torsional stiffness. For a sufficiently flexible wing, one could operate in the postclassical reversal regime, that is, $\lambda > \lambda_R|_{r=0}$, for virtually the entire range of flight conditions. Of course, divergence (or flutter) considerations may limit this option. Whether this option will prove attractive remains a subject for future investigation.

Actuator Considerations

Implementation of an aeroelastic wing with leading- and trailing-edge control surfaces requires aeroservoelastic control. Current systems include hydraulics, as well as electromechanical drives incorporating dc motors with appropriate gearing systems required to achieve the desired control surface stroke. For uninhabited aerial vehicles and uninhabited combat aerial vehicles, methods of implementing continuous (spatially deforming) as opposed to discrete control surfaces are desired to reduce radar signature and to configure control surface actuation as a function of mission requirements. As shown in the results presented, it is possible to maintain the rolling effectiveness as a function of dynamic pressure through the use of a leading-edge control surface. A schematic diagram of the conceptual control surfaces is provided in Fig. 4. As illustrated, the leading-edge control surface serves to provide an aerodynamic moment on the wing that counteracts the adverse effect of the aerodynamic moment introduced by the trailing-edge control surface when used to increase lift. If the overall deflection of the leading edge is constrained to some finite value (a requirement for practical implementation), then the trailing-edge control surface can be reversed at a point before compromising the roll effectiveness of the vehicle. It is then possible to reverse the leading- or trailing-edge control surface at a given dynamic pressure and to maneuver the vehicle beyond the conventional control surface reversal condition.

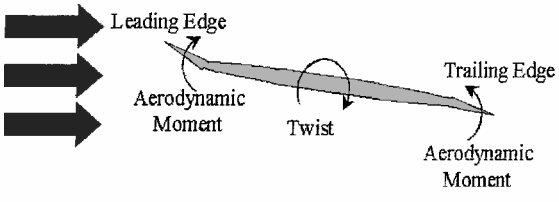

Fig. 4 Schematic diagram of control surfaces and resulting moments.

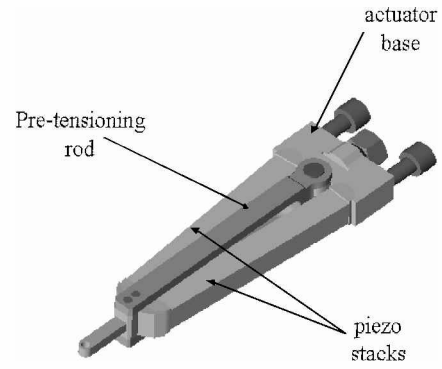

Fig. 5 Schematic of V-stack actuator.

The dynamic control of the leading- and trailing-edge control surfaces, whether they be discrete, as illustrated in the two-dimensional schematic of Fig. 5, or continuously distributed over the span of the wing, must be synchronously controlled. New actuation technologies are currently under development for high-bandwidth actuation, leveraging high-energy density materials such as piezoceramics. Two such actuation technologies include the X-frame actuator developed at the Massachusetts Institute of Technology,[16] and the V-stack actuator developed at Duke University.[17] Stroke amplification on the order of a factor of 10 can be achieved, and the actuators can be impedance matched for the desired application of dynamic load. The V-stack actuator (Fig. 5) can be readily modified for impedance matching applications by simply removing the actuator base and modifying the separation distance between the two piezoelectric stacks by increasing or decreasing the dimension of the actuator base. The current prototype actuator has a total mass of 0.65 kg, produces a force of 556 N with a tip deflection of ± 1.5 mm, a frequency response extending to approximately 600 Hz, and a mass efficiency of approximately 15%.

Such actuation devices can be integrated as a function of span to control segments of a continuously distributed control surface, both on the leading and trailing edge of the wing. Such actuation technologies can be used for dynamics associated with aircraft maneuvers as well as aeroelastic control.

Finally, it is possible that the oscillation of a leading-edge control surface may be used to create a favorable effect on such dynamic phenomena as vortex breaking or bursting. See Ref. 18 for a relevant experimental study. To assess this possibility will require a full dynamic, aeroelastic model and analysis, of course, and is well beyond the scope of this paper.

Conclusions

A leading-edge control surface may be used to counteract the tendency of a trailing-edge control surface to undergo aeroelastic reversal. Results obtained here from simple mathematical models support results obtained in more complex models including flight-test and wind-tunnel results.[3–10] An attractive control strategy to program the leading- and trailing-edge control surface rotations with flight condition has been suggested.

Moreover, the effect of the roll degree of freedom to increase the dynamic pressure at which aeroelastic divergence occurs is emphasized. This suggests it may be of interest to include the roll degree of freedom in the study of other aeroelastic phenomena including (antisymmetric) flutter.

Acknowledgments

The authors would like to thank Frank Eastep, Jay Kudva, Brian Sanders, Terry Weisshaar, and Rudy Yurkovich for helpful discussions of the literature and insights not yet reported in the literature.

References

[1] Bisplinghoff, R. L., Ashley, H., and Halfman, R. L., *Aeroelasticity*, Addison Wesley Longman Reading, MA, 1955, pp. 460–474.

[2]Dowell, E. H., Crawley, E. F., Curtiss, H. C., Jr., Peters, D. A., Scanlan, R. H., and Sisto, F., *A Modern Course in Aeroelasticity*, 3rd ed., Kluwer, Dordrecht, The Netherlands, 1995, pp. 25–41.

[3]Noll, T. E., and Eastep, F. E., "Active Flexible Wing Program," *Journal of Aircraft*, Vol. 32, No. 1, 1995, p. 9.

[4]Woods-Vedeler, J. A., Pototzky, A. S., and Hoadley, S. T., "Rolling Maneuver Load Alleviation Using Active Controls," *Journal of Aircraft*, Vol. 32, No. 1, 1995, pp. 68–76.

[5]Andersen, G., Forster, E., Kolonay, R., and Eastep, F., "Multiple Control Surface Utilization in Active Aeroelastic Wing Technology," *Journal of Aircraft*, Vol. 34, No. 4, 1997, pp. 552–557.

[6]Zink, P. S., Mavris, D. N., Love, M. H., and Karpel, M., "Robust Design for Aeroelastically Tailored/Active Aeroelastic Wing," AIAA Paper 98-4781, Sept. 1998.

[7]Weisshaar, T. A., Duke, D. K., and Dobbins, A., "Active Aeroelastic Tailoring with Adaptive Continuous Control Surfaces," AIAA Paper 2000-1619, 2000.

[8]Flick, P. M., and Love, M. H., "The Impact of Active Aeroelastic Wing Technology on Conceptual Aircraft Design," Research and Technology Organization Air Vehicle Technology Specialists Meeting on Structural Aspects of Flexible Aircraft Control, Paper RTO MP-36, Oct. 1999.

[9]Yurkovich, R. R., "Optimum Wing Shape for an Active Flexible Wing," Proceedings of the AIAA/ASME/ASCE/ARS 36th Structures, Structural Dynamics, and Materials Conference, AIAA-95-1220, 1995.

[10]Pendleton, E., Lee, M., and Wasserman, L., "Application of Active Flexible Wing Technology to the Agile Falcon," *Journal of Aircraft*, Vol. 29, No. 3, 1992, pp. 444–451.

[11]Pendleton, E., Bessette, D., Field, P., Miller, G., and Griffin, K., "Active Aeroelastic Wing Flight Research Program: Technical Program and Model Analytical Development," *Journal of Aircraft*, Vol. 37, No. 4, 2000, pp. 554–561.

[12]Kuethe, A. M., and Chow, C.-Y., *Foundations of Aerodynamics: Bases of Aerodynamic Design*, Wiley, New York, 1986, pp. 151–153.

[13]Dowell, E. H., and Hall, K. C., "Modeling of Fluid–Structure Interaction," *Annual Review of Fluid Mechanics*, Vol. 33, 2001, pp. 445–490.

[14]Hancock, G. J., "The Static Aeroelastic Deformation of Slender Configurations. Part I: Some Elementory Concepts of Static Deformation," Slender Plate Aircraft, Including Nonlinear Aerodynamics," *Aeronautical Quarterly*, Vol. 65, Aug. 1961, pp. 293–308.

[15]Hancock, G. J., "The Static Deformation of Slender Configurations. Part II: Some Calculations on Slender Plate Aircraft, Including Nonlinear Aerodynamics," *Aeronautical Quarterly*, Vol. 65, Nov. 1961, pp. 372–394.

[16]Prechtl, E. F., and Hall, S. R., "Design of a High Efficiency, Large Stroke, Electromechanical Actuator," *Journal of Smart Materials and Structures*, Vol. 8, No. 1, 1999, pp. 13–30.

[17]Ardelean, E., and Clark, R. L., "V-stack Piezoelectric Actuator," *Proceedings of the SPIE*, Vol. 4333, Smart Structures and Materials, Society of Photo-Optical Instrumentation Engineers, Bellingham, WA, 2001, pp. 322–333.

[18]Sahin, B., Akilli, H., Lin, J.-C., and Rockwell, D., "Vortex Breakdown–Edge Interaction: Consequence of Edge Oscillations," *AIAA Journal*, Vol. 39, No. 5, 2001, pp. 865–876.